An Application of the A'WOT Analysis for the Management of Cultural Heritage Assets: The Case of the Historical Farmhouses in the Aglié Castle (Turin)

A computational workflow to study particle transport and filtration in porous media: coupling CFD and deep learning

Agnese Marcato[a], Gianluca Boccardo[a,*], Daniele Marchisio[a]

[a]*DISAT - Dipartimento Scienza Applicata e Tecnologia, Politecnico di Torino, C.so Duca degli Abruzzi 24, 10129 Torino, Italy*

Abstract

In this work we developed an open-source work-flow for the construction of data-driven models from a wide Computational Fluid Dynamics (CFD) simulations campaign. We focused on the prediction of the permeability of bidimensional porous media models, and their effectiveness in filtration of a transported colloidal species. CFD simulations are performed with `OpenFOAM`, where the colloid transport is solved by the advection-diffusion equation. A campaign of two thousands simulations was performed on a HPC cluster, the permeability is calculated from the simulations with Darcy's law and the filtration (i.e. deposition) rate is evaluated by an appropriate upscaled parameter. Finally a dataset connecting the input features of the simulations with their results is constructed for the training of neural networks, executed on the open-source machine learning platform `Tensorflow` (integrated with `Python` library `Keras`). The predictive performance of the data-driven model is then compared with the CFD simulations results and with traditional analytical correlations.

Keywords: CFD, Machine learning, Porous media, Neural networks, `OpenFOAM`, `Tensorflow`

*Corresponding author
Email address: `gianluca.boccardo@polito.it` (Gianluca Boccardo)

1. Introduction

The transport of colloids in porous media, such as engineered nanomaterials, viruses, bacteria and fine powders, is a field of research that involves many different applications, from process engineering to environmental engineering and medical sciences [1]. The comprehension of this phenomenon is important, for example, for particle filtration [2, 3, 4], for the recovery of valuable colloidal materials [5, 6, 7], for catalytic processes carried in porous beds [8, 9, 10, 11, 12], for the removal of airborne colloids through air filtration in industrial and consumer services [13, 14], for the prediction of contamination of soils by pathogenic biological material [15, 16, 17] and for water and waste-water treatment [18, 19, 20]. In relation to the last application proposed, the injection of colloidal nanoscale zerovalent iron (NZVI) is a valuable technology for the remediation of contaminated aquifer systems [21, 22]. In our work we focused particularly on some of the above-mentioned applications.

The mathematical modeling of flow and transport of colloids through porous media is scientifically interesting and is needed for making predictions (for example, the filtration performance of a certain medium) and for optimization purposes. In order to obtain practically employable porous media models at the process scale (i.e. macroscopic case), it is necessary to avoid the simultaneous full characterization at the microscopic level. The relevant phenomena are thus first investigated in detail, and appropriate sub-models are subsequently extracted by means of volume averaging and homogenization techniques. In this work we focused on filtration by deposition of colloids on the grains of the porous medium due to Brownian motion regulated transport. Computational fluid dynamics (CFD) simulations can be performed in order to solve the main transport equations resulting in detailed models of the phenomena considered for the proposed geometries [23, 24].

CFD simulations were proposed for filtration applications, such as filtration in fibrous media [25, 26, 27] and particulate filters [28, 29], reactors modeling [30, 31, 32, 33, 34] and for colloids deposition in bidimensional [35, 36] and three

dimensional porous media [37], just to cite a few examples.

CFD simulations are usually computationally expensive and time consuming, this is the reason why the realization of data-driven models could be a valid surrogate of traditional physics-based models, in fact, they are able to speedily predict an output, after an appropriate training procedure. Machine Learning (ML) algorithms are able to grasp the relations that intervene between the input features for the prediction of output parameters. The gain in velocity of these models may be exploited in multiscale modeling, in-line control and parameters optimization for efficient design; developing adequate ML surrogate models is therefore a key part in the construction of effective and interoperable modelling workflows, an ever more important objective in the development of workflow management systems [38]. Specifically CFD simulations can be employed for the creation of the dataset aimed to the training of ML algorithms, i.e. establishing the "ground truth" of the data-driven model.

In the last decade ML algorithms spread in the scientific research thanks to the ability to find connections between data points that can be hardly evaluated by first-principle methods: in this way the data can be processed at higher velocity and useful informations can be extracted from them [39, 40, 41, 42, 43]. Modern ML tools can be used to improve and speed-up the relation of relevant parameters in first-principle methods such as molecular dynamics simulations [44, 45, 46]. In particular, artificial neural networks (ANN) are one of the most well-known ML tool, experiencing constant improvement and use in industry [47, 48, 49, 50].

Data-driven models have been coupled with CFD models for the prediction of fluid dynamics properties [51, 52, 53] and for the optimization of devices, for example separators [54, 55] and chemical reactors [56, 57, 58, 59]. In the case of porous media the random nature of the geometries led to the application of neural networks for the prediction of geometrical parameters: especially coupled with Lattice Boltzmann methods for the prediction of the permeability [60, 61, 62]. CFD finite volumes methods coupled with ML algorithms have not been deeply explored yet and the prediction of a wide number of fluid dynamic

parameters is an open field of research.

Thus, in this paper we propose an open-source workflow for the prediction of the permeability of bidimensional models of porous media together with their filtration performance with respect to a transported colloid (by its deposition on the porous medium surface). The construction of data-driven models for the prediction of the filtration performance is a new and innovative result that has never been proposed before. The methodology adopted can be summarized as follows: as a first step the CFD model is set up, then some geometric parameters and operating conditions are chosen as features and a thousand simulations are performed with those features ranging in established boundaries. After the permeability and the deposition rate are calculated for every simulation, a dataset is created: each simulation is expressed as a sample composed of the input features and the corresponding results. The neural network is trained with a portion of the dataset and the performance is evaluated on the remaining part (following the usual split between training and testing/validation datasets). Finally the neural network predictive efficacy of the permeability and the deposition rate is compared with some traditional analytical correlations that link those outputs with the chosen input features.

The CFD simulations are performed with the open-source toolbox `OpenFOAM 6` on a HPC cluster. The simulations setup and the dataset creation has been managed with `Python 2.7` and the neural network models have been created, trained and tested with the open-source ML framework `Tensorflow`, together with the `Python` library `Keras`.

2. Methods

2.1. Governing equations: physics-based models

The physics-based model is realized by solving the appropriate transport equations via the setup of CFD simulations. Indeed, the first thing to be noted is that the continuum hypothesis for the fluid is valid as the length scale of the porous media is in the order of hundreds of μm. First the continuity equation,

Eq. (1), and the Navier-Stokes equation, Eq. (2), are solved under the hypothesis of incompressible fluid and constant density in order to estimate the pressure and velocity fields:

$$\frac{\partial U_i}{\partial x_i} = 0, \tag{1}$$

$$\frac{\partial U_i}{\partial t} + U_j \frac{\partial U_i}{\partial x_j} = -\frac{1}{\rho}\frac{\partial p}{\partial x_i} + \nu \frac{\partial^2 U_i}{\partial x_j^2}, \tag{2}$$

where U_i is the i^{th} component of the velocity, p is the pressure, ρ is the fluid density and ν is the kinematic viscosity. As well-known, when Eq. (2) is normalized and made dimensionless the Reynolds number (Re) appears.

The transport of the colloid is modeled with the continuum approach, being the particles size four orders of magnitude smaller than the solid grains, and Fick's law is considered valid for the description of the diffusive flux because the colloid concentration in the fluid is low. As mentioned, in this study we consider the practical application of fixed dimension colloidal particles injection in water-saturated porous media. As such, considering particle density lower than 1000 kg m^{-3}, and particle size smaller than 1 μm, the resulting Stokes number is lower than unity for all the operating conditions here described. Because of this, the particles are assumed to move together with the fluid at the same velocity, and the colloid diffusion coefficient is considered constant in space; this assumption still holds close to the solid grains surface as the interactions due to attractive London forces are counterbalanced by hydrodynamic retardation effects [35, 63, 64]. Therefore the advection diffusion equation, Eq. (3), is solved for the evaluation of the concentration field:

$$\frac{\partial C}{\partial t} + U_j \frac{\partial C}{\partial x_j} = \frac{\partial}{\partial x_j}\left(\mathcal{D}\frac{\partial C}{\partial x_j}\right). \tag{3}$$

where C is the colloid concentration and $\mathcal{D}$ is the diffusion coefficient of the colloid, that is estimated by the Einstein equation:

$$\mathcal{D} = \frac{k_B T}{3\pi\mu d_P}, \tag{4}$$

where k_B is the Boltzmann constant, T is the temperature, μ is the dynamic viscosity of the fluid, and d_P is the dimension of the colloid particles. When Eq. (3) is normalized and made dimensionless the Pèclet number (Pe = Re Sc) appears. As we want to study a filtration process in its early stages (so called "clean-bed" filtration), an instantaneous reaction on the surface of the solid grains was considered, and implemented as described in the next section.

The solution of these macroscopic equations, Eqs. (1)-(3), leads to the fields mentioned before, which it is advisable to transform in more practically employable upscaled parameters. The flow field data is exploited for the evaluation of the permeability, k, that characterizes flow in saturated porous media and is calculated with the Darcy equation:

$$\frac{\Delta P}{L} = \frac{\mu}{k} q, \tag{5}$$

where ΔP is the pressure drop across the medium, L is the length of the medium in the direction of the fluid flow and q is the superficial velocity of the fluid. The Darcy equation is valid for very small values of the superficial velocity, i.e. laminar regime and Reynolds number lower than unity (Re $\ll$ 1). The colloid concentration field is instead employed for the estimation of an averaged deposition rate, K_d, which was derived by volume averaging of the advection-diffusion equation in steady state conditions and under the hypothesis that the overall source term can be expressed as the product of a macroscopic effective term and the average concentration (or in other words, by a first-order reaction), as it was derived in [65], leading to:

$$K_d = \frac{F_{tot}^{in} - F_{tot}^{out}}{\langle C \rangle V}, \tag{6}$$

where F_{tot} is the total flux (advective and diffusive) in the inlet and in the outlet, $\langle C \rangle$ is the volume average concentration of the colloid, V is the total volume of the medium.

2.2. Neural networks: data-driven models

Artificial neural networks are machine learning algorithms suited for multi-variable non-linear problems. The design of an appropriate architecture is a key point in the construction of the algorithm; generally it consists of an input layer, with a number of neurons equal to the number of inputs, one or more hidden layers, with a selected number of neurons, and an output layer, consisting of one single neuron in the case of regression problems. The input layer neurons collect the values of the input variables and send each of them to each neuron of the hidden layer, every neuron multiplies the input values by the weight, $w_{i,j}$, sums them and applies an activation function, as it is expressed in Eq. (7) for a generic neuron j. The output of each neuron is transferred as new input to the neurons in the next layer:

$$y_j^{(k)} = f\left(b_{k-1} + \sum_{i=1}^{m_{k-1}} w_{i,j}^{(k)} y_i^{(k-1)}\right), \tag{7}$$

where y_j is the output of the j^{th} neuron of the k^{th} layer, m_{k-1} is the number of neurons in the previous layer, $w_{i,j}^k$ is the weight associated to the i^{th} neuron of the previous layer, b_{k-1} is the bias of the previous layer and f is the activation function. One of the most common activation functions is the Rectified Linear Unit (ReLU):

$$\mathrm{ReLU}(z) = \max(0, z) \tag{8}$$

These kinds of feed-forward neural networks are trained by the backpropagation method, that is an iterative optimization algorithm able to adjusts the weights in order to minimize the error, usually defined as mean square error (MSE):

$$\mathrm{MSE} = \frac{1}{n}\sum_{i=1}^{n}\left(\hat{y}_i - y_i^{(k_{out})}\right)^2 \tag{9}$$

where n is the number of samples used during training and $\hat{y}_i$ is the true output. For each iteration (t) weights and biases are updated in the steepest descending

direction of the MSE function, i.e. the gradient of the MSE:

$$w_{i,j}^{(k)}(t+1) = w_{i,j}^{(k)}(t) - \lambda \frac{\partial \mathrm{MSE}}{\partial w_{i,j}^{(k)}} \tag{10}$$

where λ is the learning rate. The hyper-parameter tuning is a central issue in the creation of the data driven model: it is necessary to find out the best value of learning rate, number of hidden layers, number of neurons per layer and the best optimizer for the optimal performance of the model. The training of the ANN is performed on a certain percentage of the entire dataset, the 90 % in this work, the training set, the remaining part is the test set and is exploited for the evaluation of the performance of the model. The training stops when a fixed number of settled epochs is reached or when the MSE decreases below an established threshold.

2.3. Computational details

The workflow for the application of machine learning methods, i.e. ANN, for the prediction of fluid dynamics properties consists in three main steps. At first the construction of the CFD model, in particular the setup of the geometry and of the spatial discretization, the choice of the most appropriate solvers and boundary conditions for the resolution of Eqs. (1)-(3). Then the main operating conditions and geometry parameters are selected as predictors and a range of variation of those is established, subsequently a selected number of simulations chosen inside that range are performed. The results are than used for the calculation of the fluid dynamics properties chosen as objective of the modeling, i.e. Eqs. (5)-(6). Hence the dataset is created and it is employed for the training of the data driven model.

2.3.1. CFD model setup

We considered a simplified bi-dimensional model for a porous medium, represented by a square area containing non-overlapping circles placed randomly in order to obtain a geometry which is periodic in the direction orthogonal to

the main flow direction, i.e. the circles that cross the upper boundary are completed in the lower part of the domain, and viceversa; this is shown in Figure 1. Both monodisperse, Figure 1(a), and polydisperse, Figure 1(b), grain diameter distributions are considered. The dimension of the computational domain, as the number of grains, is established as a result of a representative elementary volume (REV) study, required for the evaluation of the minimum number of grains to whom a certain property uniquely correspond: the porosity, in this study [66, 67]. A wide field is created, then areas with an increasing number of grains are considered and the porosity is calculated. As Figure 2(a) shows, we can consider a REV constituted by 100 elements in the monodisperse case and 150 for the polydisperse one, Figure 2(b). The spatial discretization is set imposing a minimum number of cells per diameter. In case of monodisperse distributions 20 cells per diameter, in case of polydisperse distributions 10 cells per minimum diameter of the distribution, corresponding to 30 cells per mean diameter, Table (1). Grid independence studies for analogous phyisical systems can be found in our previous works [35, 37]. The geometry and the mesh are constructed with the mesh generators `blockMesh` and `snappyHexMesh`.

The system is considered isothermal at temperature equal to 298 K, the fluid is Newtonian with density equal to 997 kg m^{-3} and kinematic viscosity equal to 0.89 $\times 10^{-6}$ m^2 s^{-1}, equal to pure water viscosity at ambient temperature. The fluid flows in laminar conditions, in fact, the Reynolds number does not exceed 0.015, so no turbulence models are required in the simulations. The gravity is not considered in this model. The solver `simpleFoam` is employed for the resolution of Eqs. (1-2). The boundary conditions set on the grains surface are no-slip condition for velocity, and zero gradient of pressure; on the upper and lower boundaries a cyclic boundary condition is set. A constant pressure at the inlet (the left boundary on Figure 1) and a null pressure at the outlet (the right boundary on Figure 1) are imposed, as to obtain a fully developed velocity profile entering the porous medium.

The colloid transport is modeled as a scalar transport of the normalized particle concentration C, thus the `scalarTransportFoam` solver is employed

for the resolution of Eq. (3) in steady state conditions. A normalized inlet concentration equal to 1 and a zero gradient of the concentration are imposed as boundary conditions at the inlet and at the outlet of the porous medium respectively; a cyclic boundary condition is set at the upper and lower boundaries. On the grains surface a null concentration is imposed, representing the clean-bed filtration described earlier.

The convergence criteria on the residuals are settled as follows: 10^{-6} for the pressure, 10^{-5} for the velocity, 10^{-6} for the scalar. Concerning the discretization schemes, for the flow field evaluation they are the default second order schemes suggested by OpenFOAM 6, for the concentration field evaluation the default schemes have been changed into limited second order discretization schemes to force the concentration to range between 0 and 1.

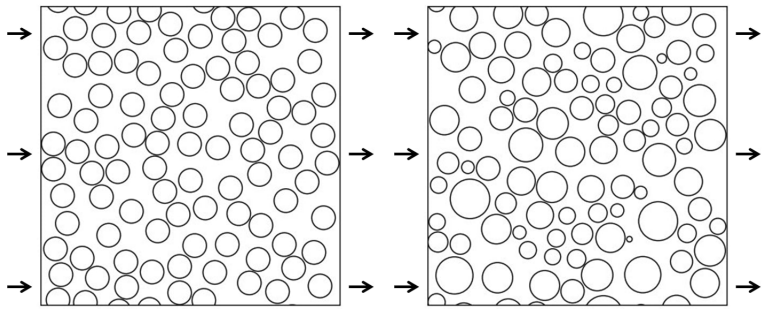

Figure 1: Sample of geometries considered in the simulation of flow and transport in porous media. Left: monodisperse geometry; right: polydisperse geometry.

2.3.2. Dataset creation

In order to produce an adequate number of samples for the training of a neural network it is necessary to automate the resolution of a large number of simulations. To that end Python scripts are realized for the automatic setup of the simulations, for checking their successful output and for the extraction of the results. The simulations are performed on a HPC cluster equipped with 29 nodes with CPU 2x Intel Xeon E5-2680 v3 2.50 GHz 12 cores. The realization of the CFD model presented in the previous paragraph allows the creation of

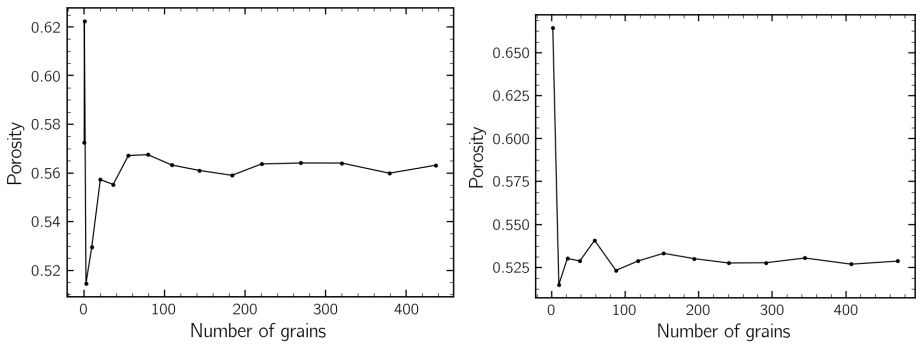

Figure 2: Representative elementary volume (REV) study: evaluation of the porosity as a function of the number of grains considered in the computational domain. Left: monodisperse geometry; right: polydisperse geometry.

a simulation template employed for the setup of all the other simulations that differ for selected parameters. Those are operating conditions and geometric parameters, in particular: the inlet pressure of the fluid, p, the size of the colloidal particles, d_c, the diameter of the grains, d_g, the porosity of the medium, ε and, just for the polydisperse geometry cases, the standard deviation of the grain diameter distribution, σ. In Table 1 the ranges of variation of those parameters are resumed. The simulations are set up with a random combination of the parameters whose values are uniformly extracted from the ranges of Table 1.The parameters are selected randomly, and not systematically, for each simulation in order to explore in the dataset the effect of a combination of parameters as wide as possible and reduce the bias in the model.

Every simulation's computational domain dimension is the same and the number of grains, i.e. the circles, is chosen as to guarantee the geometric parameters assigned, and to guarantee a suitable REV in the case of both largest porosity and grain diameter, thus having a valid REV for every other simulation.

One thousand simulations are performed for both the monodisperse and polydisperse cases, the total number of samples available for the training of the data-driven model is 962 for the first case and 996 for the second case. Less than the 4% is lost because some simulations did not reach the convergence criteria established for the CFD model.

Parameter	Range of variation	
p	0.0836 - 0.50	Pa
d_g	100 - 200	μm
σ	0.1 - 0.3	(-)
ε	0.5 - 0.65	(-)
d_c	30 - 100	nm

Table 1: Range of variation of the parameters selected as predictors for the setup of the simulations.

2.3.3. Neural network setup

The data-driven models constructed in this work are trained with the dataset created as it is described in the previous paragraph. The porosity of the porous medium, the mean grain diameter and the standard deviation of the grain distribution, for just the polydisperse case, are the predictors for the evaluation of the permeability of the medium, calculated by the Darcy equation, Eq.(5). The geometric parameters, the inlet pressure of the fluid, and the colloid dimension are the predictors for the evaluation of the deposition rate, Eq. (6). Every sample fed to the neural network training algorithm is the result of a CFD simulation performed with a different set of these predictors.

The neural network is trained with the Adam optimizer until the maximum number of epochs is reached, 20000, or when the MSE on the test set remains unchanged for a number of epochs equal to 1500. Different learning rates were employed in order to evaluate the value corresponding to the best performance of the ANN, in particular the following values of λ were tested: $10^{-1}, 10^{-2}, 10^{-3}, 10^{-4}, 10^{-5}$. Different architectures of the ANN were also tested, starting from a shallow network composed by a single hidden layer with 32 neurons, then hidden layers are added with an increasing number of neurons: 64, 128, 256. In APPENDIX A it is possible to find the detailed description of the script we developed for the implementation of the neural networks model.

The performance of the model is evaluated on the test set of the dataset, for every sample of this set the relative error between the CFD result and the

model prediction is calculated, Eq. (11). Then, the average error of the neural network is calculated as the average of the error on each sample, the different architectures and learning rate tested are compared on the basis of the average error, the maximum error and the standard deviation of the error on the test set.

$$\text{Error} = \frac{\hat{y} - y(\text{CFD})}{y(\text{CFD})}. \tag{11}$$

The hyper-parameters evaluated in this study are the learning rate and the neural network architecture, the best combination of the two for each result (permeability of the medium and deposition rate of the colloid) and for each system (monodispersed and polydisperse grain diameter distribution) is researched resulting in four different ANNs. The choice is made based on the lowest average relative error on the test set. In Figure 3 the average relative error as a function of the learning rate for the four different architectures is reported. For the prediction of the permeability of the porous medium in the monodisperse case the learning rate is chosen equal to 10^{-1} and the architecture of the ANN is $\{32\ 64\}$, i.e. two hidden layers with respectively 32 and 64 neurons. For the prediction of the permeability of the porous medium in the polydisperse case the learning rate is chosen equal to 10^{-3} and the architecture of the ANN is $\{32\}$, i.e. one hidden layer with 32 neurons. For the prediction of the deposition rate of the colloid in the monodisperse case the learning rate is chosen equal to 10^{-2} and the architecture of the ANN is $\{32\ 64\ 128\}$, i.e. two hidden layers with respectively 32, 64 and 128 neurons. For the prediction of the deposition rate of the colloid in the polydisperse case the learning rate is chosen equal to 10^{-2} and the architecture of the ANN is $\{32\ 64\}$, i.e. two hidden layers with respectively 32 and 64 neurons.

3. Results and discussion

In this section the results of the CFD simulations are presented and both analytical and data-driven models are proposed for the prediction of the upscaled parameters described before, namely permeability k and reaction rate $\mathrm{K_d}$.

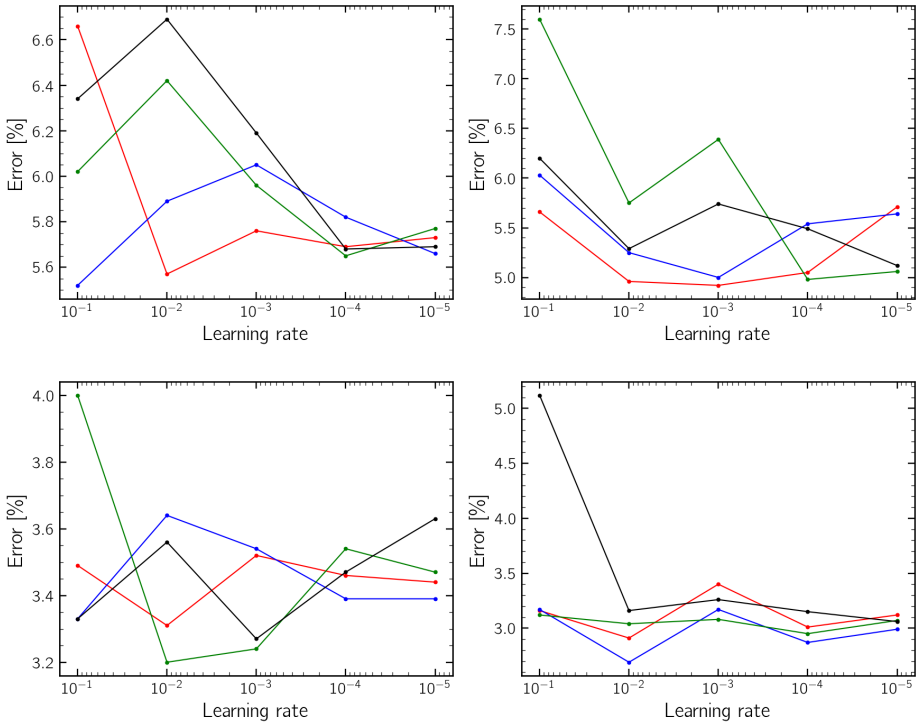

Figure 3: Hyperparameter tuning of the neural network: mean relative error on the test set as a function of the learning rate (10^{-1}, 10^{-2}, 10^{-3}, 10^{-4}, 10^{-5}) and of the network architecture ({32} in red, {32, 64} in blue, {32, 64, 128} in green, {32, 64, 128, 256} in black, refer to the end of section 2 for the bracket nomenclature). Top: error on the prediction of permeability; bottom: error on the prediction of deposition rate; left: monodisperse grains; right: polydisperse grains.

3.1. Flow field results

$$\frac{\Delta P \rho}{G_0^2}\frac{d_g}{L}\frac{\varepsilon^3}{(1-\varepsilon)} = 150\frac{1-\varepsilon}{(d_g G_0)/\mu} + 1.75, \tag{12}$$

where G_0 is the mass flux, $G_0 = \rho q$. The inertial term of the Ergun equation in the cases of this work is negligible since all the samples fall in laminar regime. The results obtained from the simulations are not completely in agreement with the equation because the geometries are bi-dimensional whereas Ergun's equation is valid for three-dimensional packed beds. Similar results were obtained in our past work [35] for a smaller number of simulations performed. The polydisperse geometries, referring to the polydisperse grains, deviate less from the

theoretical equation compared to monodisperse ones, moreover the higher is the standard deviation of the grain diameter distribution the lower is this deviation, Figure 4(b). This behavior can be explained considering that the most likely bi-dimensional description of a monodisperse 3D porous medium is a 2D polydisperse geometry. In fact, if we imagine to cut with a surface a three-dimensional sphere arrangement in the flow direction we obtain circles with different diameter and most of them will not be in contact. Two contour plots for a qualitative description of the flow field are presented in Figure 5, where the fluid flows from left to right and it is possible to appreciate the presence of the periodic boundary conditions on the upper and lower boundaries.

The permeability is the first upscaled parameter we have approached for testing the workflow proposed in the previous section. It is a well known descriptor of a porous medium from the geometrical point of view, and in our case it is calculated by comparing the results of the CFD simulations with Darcy's law, Eq. (5). The Kozeny equation, $k = C_k \frac{\varepsilon^3}{(1-\varepsilon)^2 M_s^2}$ where M_s is the specific surface of the porous medium (m^2/m^3), instead is an expression for the permeability that depends just on geometrical parameters: it is exploited as an analytical model to compare with the results of the data-driven model. The Kozeny constant is evaluated by fitting of the CFD results, Figure 6, resulting in C_k equal to 0.084 for both monodisperse and polydisperse geometries. The average error associated to the prediction of the permeability by the Kozeny equation, calculated according to Eq. (11), is equal to 10.1% for monodisperse geometries and 8.2% for polydisperse geometries. The error linked to the polydisperse geometries is lower than in the monodisperse case, even in this case this behavior is amenable to the most likely 3D approximation of the first ones. The specific surface has been evaluated in an analytical way starting from the radii of the grains and the dimensions of the geometries, we proved that the quality of the predictions of the Kozeny law does not change if the specific surface is evaluated from the meshed geometry.

The performance of the optimized neural networks, Figures 3(a) and 3(b), is shown in the parity diagrams of Figure 7, where the results of the CFD

	monodisperse geometries		polydisperse geometries	
	k	K_d	k	K_d
Average error	5.52%	3.24%	4.92%	2.69%
Maximum error	25.85%	10.35%	20.03%	11.99%
Standard deviation	4.43%	2.44%	3.48%	2.49%

Table 2: Performance of the neural networks.

simulations and the result of the model are compared. In Table 2 the average error, the maximum error and the standard deviation of the error are reported. The neural networks are able to predict the permeability with an average error of 5.5% and 4.92% respectively for monodisperse and polydisperse geometries, instead the Kozeny equation results in errors of 10.1% and 8.2% respectively, so the neural networks perform better with average errors about 40% lower than the traditional correlation for the geometries proposed and for the range of operating conditions explored in this work.

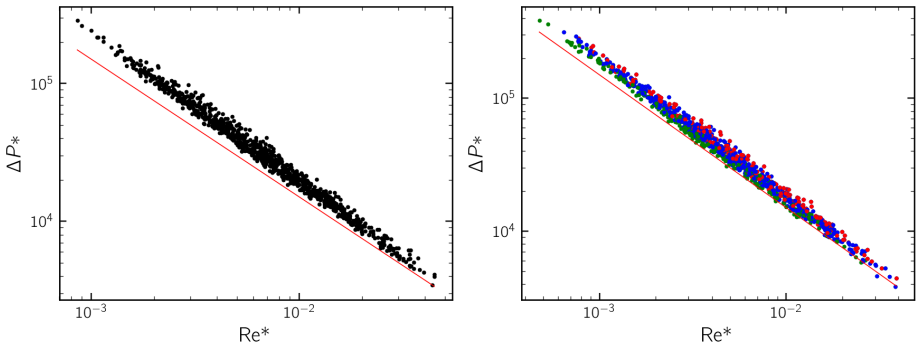

Figure 4: Comparison of CFD results (black points) with Ergun's equation (red line). Left: monodisperse geometry; right: polydisperse geometry with σ (i.e. standard deviation in diameter distribution) between 0.1 and 0.15 in green, between 0.15 and 0.25 in blue, between 0.25 and 0.3 in red.

3.2. Transport field results

After having obtained the flow field results, the particle deposition simulations are performed as described before. In Figure 8 two contour plots of the concentration at the steady state are reported. The two cases proposed differ

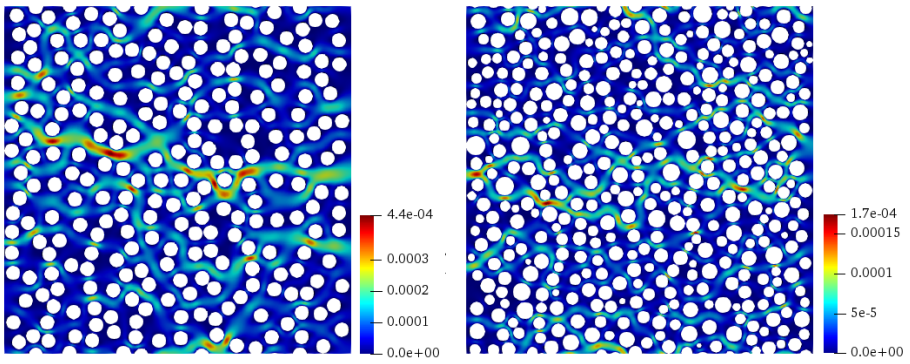

Figure 5: Contour plot of the fluid velocity (ms^{-1}), from left to right. Left: monodisperse grain distribution geometry (Re = 0.0071); right: polydisperse grain distribution geometry (Re = 0.0021).

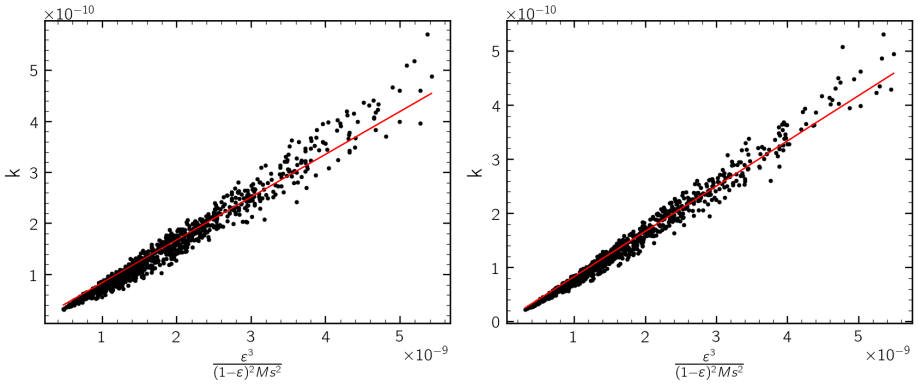

Figure 6: Evaluation of the Kozeny coefficient through linear regression. Left: monodisperse geometry; right: polydisperse geometry.

for the geometry and for the Pèclet number, defined as:

$$(Pe) = \frac{q d_g}{\mathcal{D}}. \tag{13}$$

So at high Pèclet numbers the convective term prevails on the diffusive one and as a consequence the filtering performance of the porous medium decreases, as it is apparent comparing Figure 8(a) with Figure 8(b). The time required for the resolution of each CFD simulation, considering both `simpleFoam` and `scalarTransportFoam` solvers, is 1.2 hours in the case of monodisperse grains

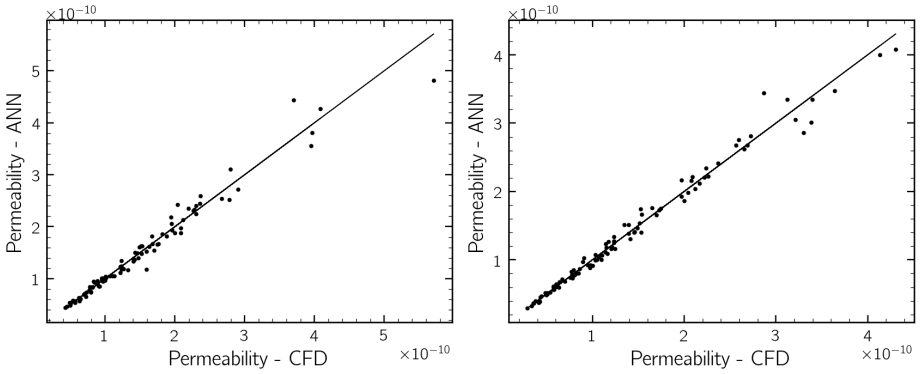

Figure 7: Parity diagrams of the permeability prediction on the test set for the optimal neural networks trained with the best hyperparameters. Left: monodisperse geometry; right: polydisperse geometry.

geometries and 4 hours in the case of polydisperse grains geometries, which have an higher number of cells.

The data-driven model we designed is aimed to the prediction of the deposition rate, K_d, as defined in the previous section, Eq. (6). From the literature [65] we know that this upscaled parameter is correlated to the Pèclet number through the Damköhler number, which in this work we define as follows:

$$\mathrm{Da} = \frac{K_d L}{q}. \tag{14}$$

The classic upscaled parameter for the evaluation of the filtration performance is the deposition efficiency η, whose best adimensional descriptor[1] is the Pèclet number [2, 68, 69]; while in this work we have chosen to employ the more reliable macroscale parameter K_d (as explained in [65], the same functional dependence holds. Thus we consider a relationship of the form:

$$\mathrm{Da} = APe^B, \tag{15}$$

The values of parameters A and B obtained from the best fit of the results

[1] if one considers only Brownian diffusion, as it is the case in this work

dataset, Figure 9, the following values are obtained: A = 6.394×10^9, B = -0.928 for the monodisperse geometry, A = 7.413×10^9, B = -0.973 for the polydisperse geometry. The average error of the prediction is equal to 12.2% for the first case and 11.9% for the second case.

The performance of the optimized neural networks, Figure 3(c) and 3(d), is evaluated in the parity diagrams of Figure 10 where all the predictions on the test set samples are reported: the average error is equal to 3.24% for the monodisperse case and 2.69% for the polydisperse case. In Table 2 more details on the data-driven models accuracy are reported. Even in this case the data-driven model is able to better predict the deposition efficiency with respect to the classical relationship structured on dimensionless number dependency. In the limit of the cases explored in the current dataset, the error associated to the predictions is one order of magnitude lower than the one correlated to the analytical correlation, Eq. 15. The neural networks training process took about 4 minutes and the trained model is able to predict almost instantly its output.

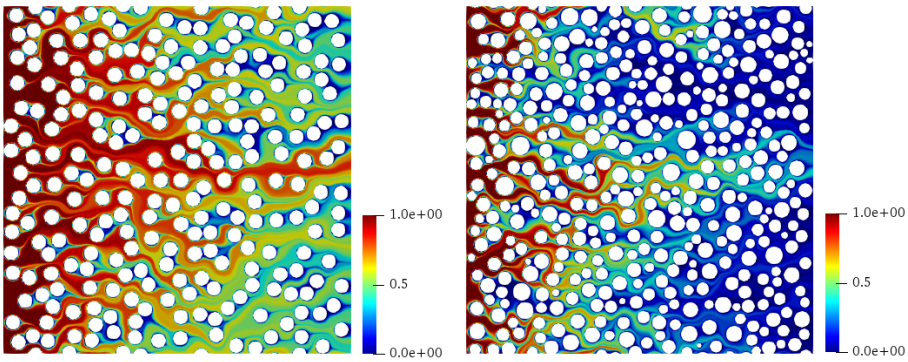

Figure 8: Contour plot of the normalized concentration. Left: Monodisperse grain distribution geometry (Pe = 990.0); right: Polydisperse grain distribution geometry (Pe = 252.5).

4. Conclusions

In this work we successfully developed an open-source workflow for the realization of a dataset starting from a campaign of CFD simulations aimed to the

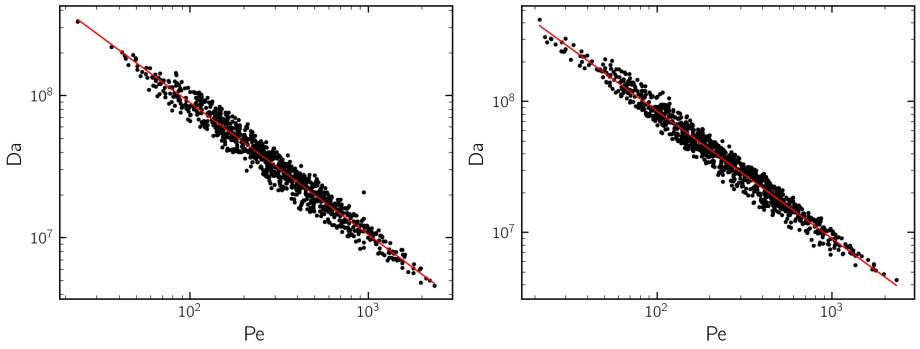

Figure 9: Evaluation of the correlation between the Damköhler number and the Pèclet number. Left: monodisperse geometry; right: polydisperse geometry.

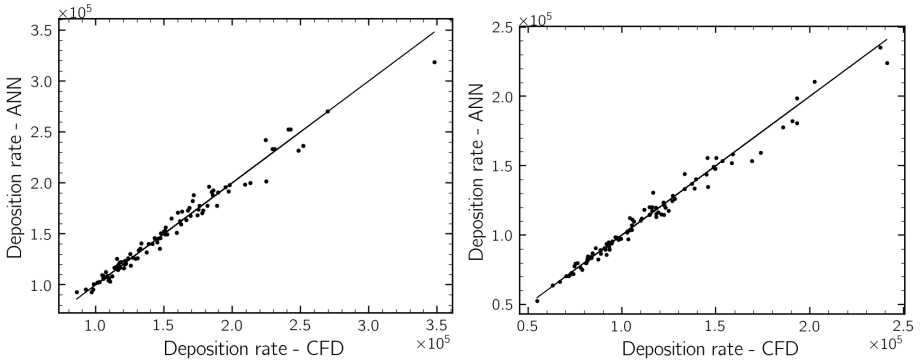

Figure 10: Parity diagrams of the deposition rate prediction on the test set for the optimal neural networks trained with the best hyperparameters. Left: monodisperse geometry; right: polydisperse geometry.

training of neural networks for the prediction of fluid dynamics quantities. Neural networks have been employed to predict the permeability and the deposition rate for the investigated cases. In conclusion:

- The average error on the test set for the permeability it is lower than 6% and for the deposition rate, which has never been predicted with machine learning tools before, is lower than 3.5% for both geometrical models;
- The networks allow the comprehension of the relations between parameters, and they also provide more accurate predictions of the permeability and the deposition rate compared to traditional analytical expressions,

with average errors lower than 40% in the range of operating conditions explored in this work;

- The data-driven models, once trained, can instantaneously give a satisfactorily accurate output, while a CFD simulation requires a certain amount of computational time. In our case each CFD simulation requires from one to four hours to be solved and the training takes four minutes. The increase in the predictive velocity can be exploited in multiscale modeling, in-line control and optimization problems;

ML algorithms, in particular neural networks, are promising tools in modeling advancement of intrinsically random problems as porous media are. To enhance the predictive accuracy new elaborated input features could be employed, such as the tortuosity and the pore size distribution, paying attention to the choice of parameters that can be experimentally evaluated. To avoid the arduous selection of parameters representing the randomness of the media, another way to solve the problem is to submit the entire geometry as training input for the neural network: in this way the algorithm itself could select the most important features in the image. In this case more sophisticated techniques must be used, such as convolutional neural networks, which will be our next research focus.

APPENDIX A - Neural network model

The neural network model has been setup as follows. At first the dataset is imported, then it is scaled between -1 and 1 using the `MinMaxScaler` function of the `Scikit-learn` library of `Python`. The scaled dataset is divided into the training and test set with a split of 90%. The architecture of the neural network is setup with `Keras` as a sequential model, where `Dense` layers are added. The loss function employed during the training is the mean square error, the Adam optimizer is used and a batch size of 50 is settled. The `ModelCheckpoint` and `EarlyStopping` callbacks of `Keras` are used for the control of the training process. The code can be found in the supplementary material.

Acknowledgments

Computational resources were provided by HPC@POLITO, a project of Academic Computing within the Department of Control and Computer Engineering at the Politecnico di Torino (http://www.hpc.polito.it). The Authors want to thank Matteo Icardi for the interesting discussions, and they also acknowledge that the project leading to this publication has received funding from the European Union's Horizon 2020 research and innovation programme under grant agreement No. 760907.

References

[1] I. L. Molnar, E. Pensini, M. A. Asad, C. A. Mitchell, L. C. Nitsche, L. J. Pyrak-Nolte, G. L. Miño, M. M. Krol, Colloid transport in porous media: a review of classical mechanisms and emerging topics, Transport in Porous Media 130 (1) (2019) 129–156.

[2] K. Yao, M. T. Habibian, C. R. O'Melia, Water and waste water filtration. concepts and applications, Environmental science & technology 5 (11) (1971) 1105–1112.

[3] O. Iliev, R. Kirsch, Z. Lakdawala, S. Rief, K. Steiner, Modeling and simulation of filtration processes, in: Currents in Industrial Mathematics, Springer, 2015, pp. 163–228.

[4] E. Crevacore, G. Boccardo, D. Marchisio, R. Sethi, Microscale colloidal transport simulations for groundwater remediation, Chemical Engineering Transactions 47 (2016) 271–276.

[5] M. A. Rabah, F. Farghaly, M. Abd-El Motaleb, Recovery of nickel, cobalt and some salts from spent ni-mh batteries, Waste Management 28 (7) (2008) 1159–1167.

[6] S. M. Shin, N. H. Kim, J. S. Sohn, D. H. Yang, Y. H. Kim, Development of a metal recovery process from Li-ion battery wastes, Hydrometallurgy 79 (3-4) (2005) 172–181.

[7] J. E. Hoffmann, Recovery of platinum-group metals from gabbroic rocks metals from auto catalysts, Journal of Metals 40 (6) (1988) 40–44.

[8] G. Boccardo, F. Augier, Y. Haroun, D. Ferre, D. L. Marchisio, Validation of a novel open-source work-flow for the simulation of packed-bed reactors, Chemical Engineering Journal 279 (2015) 809–820.

[9] S. Bensaid, D. L. Marchisio, D. Fino, G. Saracco, V. Specchia, Modelling of diesel particulate filtration in wall-flow traps, Chemical Engineering Journal 154 (2009) 211–218.

[10] S. Bensaid, D. L. Marchisio, N. Russo, D. Fino, Experimental investigation of soot deposition in diesel particulate filters, Catalysis Today 147S (2009) s295–s300.

[11] S. Bensaid, D. L. Marchisio, D. Fino, Numerical simulation of soot filtration and combustion within diesel particulate filters, Chemical Engineering Science 65 (1) (2010) 357–363.

[12] M. Behnam, A. G. Dixon, P. M. Wright, M. Nijemeisland, E. H. Stitt, Comparison of cfd simulations to experiment under methane steam reforming reacting conditions, Chemical engineering journal 207 (2012) 690–700.

[13] W. J. Fisk, D. Faulkner, J. Palonen, O. Seppanen, Performance and costs of particle air filtration technologies, Indoor Air 12 (4) (2002) 223–234.

[14] P. Biswas, C.-Y. Wu, Nanoparticles and the environment, Journal of the Air and Waste Management Association 55 (6) (2005) 708–746.

[15] S. A. Bradford, R. W. Harvey, Future research needs involving pathogens in groundwater, Hydrogeology Journal 25 (4) (2017) 931–938.

[16] T. K. Sen, Processes in pathogenic biocolloidal contaminants transport in saturated and unsaturated porous media: A review, Water, Air, and Soil Pollution 216 (2011) 239–256.

[17] S. Wang, L. Li, S. Yu, B. Dong, N. Gao, X. Wang, A review of advances in edcs and phacs removal by nanofiltration: mechanisms, impact factors and the influence of organic matter, Chemical Engineering Journal (2020) 126722.

[18] T. Tosco, J. Bosch, R. U. Meckenstock, R. Sethi, Transport of ferrihydrite nanoparticles in saturated porous media: role of ionic strength and flow rate, Environmental Science and Technology 46 (7) (2012) 4008–4015.

[19] J. Wang, Z. Yao, Y. Jiang, B. Xi, S. Ni, L. Zhang, et al., Aminated electrospun nanofiber membrane as permeable reactive barrier material for ef-

fective in-situ cr (vi) contaminated soil remediation, Chemical Engineering Journal 406 126822.

[20] Y. Gan, J. Li, L. Zhang, B. Wu, W. Huang, H. Li, S. Zhang, Potential of titanium coagulants for water and wastewater treatment: Current status and future perspectives, Chemical Engineering Journal (2020) 126837.

[21] A. Tiraferri, R. Sethi, Enhanced transport of zerovalent iron nanoparticles in saturated porous media by guar gum, Journal of Nanoparticle Research 11 (3) (2009) 635–645.

[22] F. He, D. Zhao, J. Liu, C. B. Roberts, Stabilization of Fe-Pd nanoparticles with sodium carboxymethyl cellulose for enhanced transport and dechlorination of trichloroethylene in soil and groundwater, Industrial & Engineering Chemistry Research 46 (1) (2007) 29–34.

[23] N. Agrawal, P. Nair, T. Pöschel, S. Roy, Isotropy of sphere packings in a cylindrical confinement, Chemical Engineering Journal 377 (2019) 119820.

[24] A. Srivastava, K. Nigam, S. Roy, Quantification of local structure of disordered packing of spherical particles, Chemical Engineering Journal 377 (2019) 119771.

[25] C. Yue, Q. Zhang, Z. Zhai, Numerical simulation of the filtration process in fibrous filters using cfd-dem method, Journal of Aerosol Science 101 (2016) 174–187.

[26] A. K. Maddineni, D. Das, R. M. Damodaran, Air-borne particle capture by fibrous filter media under collision effect: A cfd-based approach, Separation and Purification Technology 193 (2018) 1–10.

[27] R. Ghidossi, J. V. Daurelle, D. Veyret, P. Moulin, Simplified CFD approach of a hollow fiber ultrafiltration system, Chemical Engineering Journal 123 (2006) 117–125.

[28] I. Belot, D. Vidal, R. Greiner, M. Votsmeier, R. E. Hayes, F. Bertrand, Impact of washcoat distribution on the catalytic performance of gasoline particulate filters as predicted by lattice boltzmann simulations, Chemical Engineering Journal 406 (2020) 127040.

[29] I. Belot, Y. Sun, D. Vidal, M. Votsmeier, P. Causse, F. Trochu, F. Bertrand, A 3d additive manufacturing approach for the validation of a numerical wall-scale model of catalytic particulate filters, Chemical Engineering Journal 405 (2020) 126653.

[30] A. Jafari, P. Zamankhan, S. M. Mousavi, K. Pietarinen, Modeling and CFD simulation of flow behavior and dispersivity through randomly packed bed reactors, Chemical Engineering Journal 144 (2008) 476–482.

[31] T. Atmakidis, E. Y. Kenig, CFD-based analysis of the wall effect on the pressure drop in packed beds with moderate tube/particle diameter ratios in the laminar flow regime, Chemical Engineering Journal 155 (2009) 404–410.

[32] S. Pawlowski, N. Nayak, M. Meireles, C. A. Portugal, S. Velizarov, J. G. Crespo, CFD modelling of flow patterns, tortuosity and residence time distribution in monolithic porous columns reconstructed from X-ray tomography data, Chemical Engineering Journal 350 (2018) 757–766.

[33] L. Chen, S. Pannala, R. Broekhuis, P. Gautam, T. Gu, D. West, V. Balakotaiah, Three-dimensional cfd simulation of pattern formation in a shallow packed-bed reactor for oxidative coupling of methane, Chemical Engineering Journal 400 (2020) 125979.

[34] K. Tong, L. Yang, X. Du, Modelling of tio2-based packing bed photocatalytic reactor with raschig rings for phenol degradation by coupled cfd and dem, Chemical Engineering Journal 400 (2020) 125988.

[35] G. Boccardo, D. L. Marchisio, R. Sethi, Microscale simulation of particle

deposition in porous media, Journal of Colloid and Interface Science 417 (2014) 227–237.

[36] G. Boccardo, I. M. Sokolov, A. Paster, An improved scheme for a robin boundary condition in discrete-time random walk algorithms, Journal of Computational Physics 374 (2018) 1152–1165.

[37] G. Boccardo, R. Sethi, D. L. Marchisio, Fine and ultrafine particle deposition in packed-bed catalytic reactors, Chemical Engineering Science 198 (2019) 290–304.

[38] M. T. Horsch, C. Niethammer, G. Boccardo, P. Carbone, S. Chiacchiera, M. Chiricotto, J. D. Elliott, V. Lobaskin, P. Neumann, P. Schiffels, et al., Semantic interoperability and characterization of data provenance in computational molecular engineering, Journal of Chemical & Engineering Data 65 (3) (2019) 1313–1329.

[39] S. Makridakis, The forthcoming Artificial Intelligence (AI) revolution: Its impact on society and firms (2017).

[40] V. Venkatasubramanian, The promise of artificial intelligence in chemical engineering: Is it here, finally?, AIChE Journal 65 (2) (2019) 466–478.

[41] M. Reichstein, G. Camps-Valls, B. Stevens, M. Jung, J. Denzler, N. Carvalhais, Prabhat, Deep learning and process understanding for data-driven Earth system science, Nature 566 (7743) (2019) 195–204.

[42] X. Zhu, Z. Wan, D. C. Tsang, M. He, D. Hou, Z. Su, J. Shang, Machine learning for the selection of carbon-based materials for tetracycline and sulfamethoxazole adsorption, Chemical Engineering Journal 406 (2020) 126782.

[43] L. Li, S. Rong, R. Wang, S. Yu, Recent advances in artificial intelligence and machine learning for nonlinear relationship analysis and process control in drinking water treatment: A review, Chemical Engineering Journal 405 (2020) 126673.

[44] N. Di Pasquale, M. Bane, S. J. Davie, P. L. Popelier, Ferebus: highly parallelized engine for kriging training, Journal of computational chemistry 37 (29) (2016) 2606–2616.

[45] S. J. Davie, N. Di Pasquale, P. L. Popelier, Incorporation of local structure into kriging models for the prediction of atomistic properties in the water decamer, Journal of computational chemistry 37 (27) (2016) 2409–2422.

[46] N. Di Pasquale, S. J. Davie, P. L. Popelier, Optimization algorithms in optimal predictions of atomistic properties by kriging, Journal of chemical theory and computation 12 (4) (2016) 1499–1513.

[47] F. Noé, G. De Fabritiis, C. Clementi, Machine learning for protein folding and dynamics, Current Opinion in Structural Biology 60 (2020) 77–84.

[48] Y. Su, T. Ng, Z. Li, J. H. Davidson, Sparse scattered high performance computing data driven artificial neural networks for multi-dimensional optimization of buoyancy driven heat and mass transfer in porous structures, Chemical Engineering Journal (2020) 125257.

[49] D. Wu, D. Zhang, S. Liu, Z. Jin, T. Chowwanonthapunya, J. Gao, X. Li, Prediction of polycarbonate degradation in natural atmospheric environment of china based on bp-ann model with screened environmental factors, Chemical Engineering Journal (2020) 125878.

[50] S. Mittal, S. Pathak, H. Dhawan, S. Upadhyayula, A machine learning approach to improve ignition properties of high-ash indian coals by solvent extraction and coal blending, Chemical Engineering Journal (2020) 127385.

[51] M. M. Tafarroj, R. Daneshazarian, A. Kasaeian, CFD modeling and predicting the performance of direct absorption of nanofluids in trough collector, Applied Thermal Engineering 148 (2019) 256–269.

[52] M. Saeedan, A. R. Solaimany Nazar, Y. Abbasi, R. Karimi, CFD Investigation and neutral network modeling of heat transfer and pressure drop of

nanofluids in double pipe helically baffled heat exchanger with a 3-D fined tube, Applied Thermal Engineering 100 (2016) 721–729.

[53] Y. Ding, Y. Zhang, Y. M. Ren, G. Orkoulas, P. D. Christofides, Machine learning-based modeling and operation for ALD of SiO2 thin-films using data from a multiscale CFD simulation, Chemical Engineering Research and Design 151 (2019) 131–145.

[54] D. Park, J. Cha, M. Kim, J. S. Go, Multi-objective optimization and comparison of surrogate models for separation performances of cyclone separator based on CFD, RSM, GMDH-neural network, back propagation-ANN and genetic algorithm, Engineering Applications of Computational Fluid Mechanics 14 (1) (2020) 180–201.

[55] D. Misiulia, K. Elsayed, A. G. Andersson, Geometry optimization of a deswirler for cyclone separator in terms of pressure drop using CFD and artificial neural network, Separation and Purification Technology 185 (2017) 10–23.

[56] J. D. Smith, A. A. Neto, S. Cremaschi, D. W. Crunkleton, CFD-based optimization of a flooded bed algae bioreactor, Industrial and Engineering Chemistry Research 52 (22) (2013) 7181–7188.

[57] A. Mosavi, S. Shamshirband, E. Salwana, K. wing Chau, J. H. Tah, Prediction of multi-inputs bubble column reactor using a novel hybrid model of computational fluid dynamics and machine learning, Engineering Applications of Computational Fluid Mechanics 13 (1) (2019) 482–492.

[58] B. R. Hough, D. A. Beck, D. T. Schwartz, J. Pfaendtner, Application of machine learning to pyrolysis reaction networks: Reducing model solution time to enable process optimization, Computers and Chemical Engineering 104 (2017) 56–63.

[59] M. Babanezhad, M. Rezakazemi, N. Hajilary, S. Shirazian, Liquid-phase chemical reactors: Development of 3D hybrid model based on CFD-

adaptive network-based fuzzy inference system, Canadian Journal of Chemical Engineering 97 (S1) (2019) 1676–1684.

[60] J. Wu, X. Yin, H. Xiao, Seeing permeability from images: fast prediction with convolutional neural networks, Science Bulletin 63 (18) (2018) 1215–1222.

[61] J. Tian, C. Qi, Y. Sun, Z. M. Yaseen, B. T. Pham, Permeability prediction of porous media using a combination of computational fluid dynamics and hybrid machine learning methods, Engineering with Computers (2020) 1–17.

[62] A. Rabbani, M. Babaei, Hybrid pore-network and lattice-Boltzmann permeability modelling accelerated by machine learning, Advances in Water Resources 126 (2019) 116–128.

[63] Z. Adamczyk, T. Dabros, J. Czarnecki, T. G. Van De Ven, Particle transfer to solid surfaces, Advances in Colloid and Interface Science 19 (3) (1983) 183–252.

[64] D. C. Prieve, E. Ruckenstein, Effect of london forces upon the rate of deposition of brownian particles, AIChE Journal 20 (6) (1974) 1178–1187.

[65] G. Boccardo, E. Crevacore, R. Sethi, M. Icardi, A robust upscaling of the effective particle deposition rate in porous media, Journal of Contaminant Hydrology 212 (2018) 3–13.

[66] Y. Bachmat, J. Bear, On the concept and size of a representative elementary volume (rev), in: Advances in transport phenomena in porous media, Springer, 1987, pp. 3–20.

[67] J. Bear, Dynamics of fluids in porous media, Courier Corporation, 2013.

[68] M. Elimelech, Kinetics of capture of colloidal particles in packed beds under attractive double layer interactions, Journal of colloid and interface science 146 (2) (1991) 337–352.

[69] N. Tufenkji, M. Elimelech, Correlation equation for predicting single-collector efficiency in physicochemical filtration in saturated porous media, Environmental science & technology 38 (2) (2004) 529–536.